JOURNAL OF MATERIALS SCIENCE 24 (1989) 213–219

Sintering of Sb_2O_3-doped ZnO

JINHO KIM, TOSHIO KIMURA, TAKASHI YAMAGUCHI
Faculty of Science and Technology, Keio University, Yokohama, Japan

The effect of Sb_2O_3 on the densification of ZnO was studied and compared with that for additives such as $ZnSb_2O_6$, α-$Zn_7Sb_2O_{12}$, and Sb_2O_4. Addition of up to 2.0 mol% Sb_2O_3 raised the densification temperature of ZnO from 600° C to 1000° C regardless of doping level and the particle size of Sb_2O_3. Addition of other antimony-additives, however, slowed down the densification of ZnO, and the densification temperature increased with increasing amount of additives. Results of TG, XRD and SEM showed that the observed densification characteristics in Sb_2O_3-doped ZnO are explained by the volatile nature of Sb_2O_3. Thus, Sb_2O_3 evaporates during oxidation at about 500° C and condenses on the ZnO particle surfaces as a non-crystalline phase of an unknown composition, which checks the material transport across ZnO particles resulting in the retarded densification.

1. Introduction

Zinc oxide is an n-type semiconductor and used as gas sensors [1] and ZnO varistors [2, 3]. Generally, the mechanical and electric properties of ceramic materials are determined by their microstructures. Many attempts have been made for microstructure control by adjusting the fabrication process or sintering aids.

In ZnO, inhibition of grain growth by a small amount of K_2O [4] or Sb_2O_3 [5] and either promotion or suppression of densification by Li_2O or In_2O_3 [6–8] are reported. The effects of these additives on the sintering behaviour of ZnO have been interpreted in terms of Zener drag [9, 10] and lattice defects [11, 12].

In ZnO varistors, three phases exist during firing; ZnO, intergranular spinel phase and liquid Bi_2O_3 [13]. The grain growth of ZnO is inhibited by the spinel phase [14] but is promoted by Bi_2O_3. The spinel phase in ZnO varistors is composed mainly of ZnO and Sb_2O_3 with partially dissolved CoO and MnO [15]. Therefore, the sintering behaviour of respective binary systems such as ZnO–Bi_2O_3 and ZnO–Sb_2O_3 is important to understand the sintering mechanism in ZnO varistors.

Many studies have been done on ZnO–Bi_2O_3 binary system [16, 17]. The system ZnO–Sb_2O_3, however, has not been fully explored and most reaction studies have been done at high doping levels and in the coexistence of other dopants [18]. Antimony trioxide is known to react with ZnO to form $ZnSb_2O_6$ at about 700° C and changes to α-$Zn_7Sb_2O_{12}$ spinel phase at a higher temperature

$$ZnO + Sb_2O_3 + O_2 \rightarrow ZnSb_2O_6 \quad (1)$$

$$ZnSb_2O_6 + 6ZnO \rightarrow \alpha\text{-}Zn_7Sb_2O_{12} \quad (2)$$

To understand the effect of Sb_2O_3 on the sintering of ZnO, we need to know how the sintering of ZnO depends on the doping level of Sb_2O_3 and what reaction occurs at practical doping levels in sintering.

We studied the densification of Sb_2O_3-doped ZnO at doping levels up to 2.0 mol% and correlated the obtained results with phase changes in heating. The effect of chemical species of antimony-oxide on the densification was studied using Sb_2O_4, $ZnSb_2O_6$ and α-$Zn_7Sb_2O_{12}$.

2. Experimental procedure

2.1. Materials

Zinc oxide (99.9%) and two types of cubic Sb_2O_3 (99.8%, coarse and fine) were used as raw materials. The average particle size of ZnO determined with a centrifugal sedimentation particle analyser (CAPA-500, Horiba Co.) was 0.7 μm. The coarse and fine Sb_2O_3 powders, designated as S_c and S_f, had average particle sizes of 4.1 μm and 1.2 μm, respectively. Fig. 1 shows SEMs of raw materials. Coarse Sb_2O_3 (S_c) was well dispersed, while ZnO and fine Sb_2O_3 contained soft agglomerates.

Two compounds $ZnSb_2O_6$ and α-$Zn_7Sb_2O_{12}$ in the system ZnO–Sb_2O_3 were prepared by the following procedures. Mixtures of ZnO and fine Sb_2O_3 with the corresponding molar ratios were prepared by wet ball-milling for 5 h. They were compacted into discs and fired at 700° C for $ZnSb_2O_6$ and 1000° C for α-$Zn_7Sb_2O_{12}$ both for 10 h in oxygen [19] at a heating rate of 100° C h^{-1}. The obtained materials were named ZS and SP, respectively. Fired discs were crushed in an agate mortar and dispersed in distilled water. Each powder was treated by sedimentation to collect particles below 3 μm. Antimony tetraoxide powder (designated as S′) was obtained by heating coarse Sb_2O_3 at 600° C for 3 h in air followed by wet ball-milling for 5 h in ethanol using alumina balls. All the obtained materials were identified by X-ray powder diffraction analysis.

Zinc oxide powder was mixed with 0.1, 0.5, 1.0 and 2.0 mol% of coarse and fine Sb_2O_3 powders by wet ball-milling in ethanol using a plastic pot and balls for 10 h. Three antimony additives of ZS ($ZnSb_2O_6$), SP

0022–2461/89 $03.00 + .12

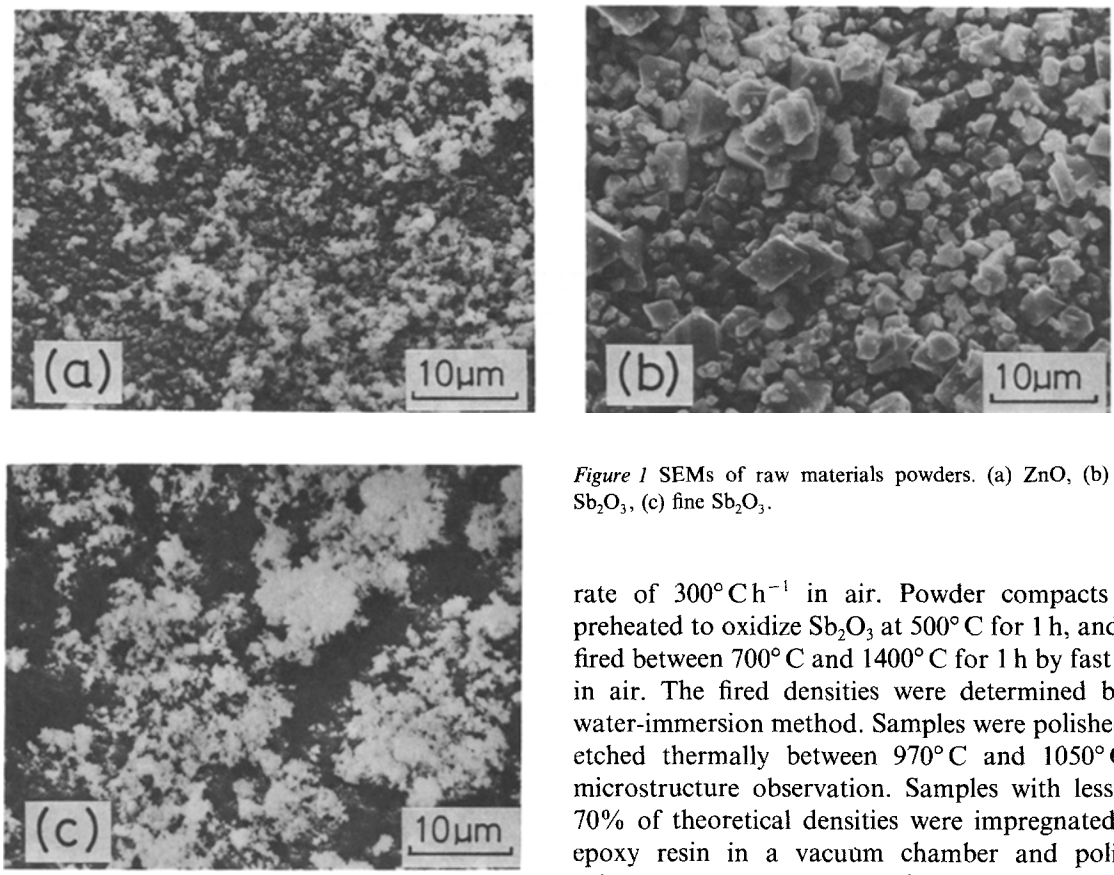

Figure 1 SEMs of raw materials powders. (a) ZnO, (b) coarse Sb_2O_3, (c) fine Sb_2O_3.

(α-$Zn_7Sb_2O_{12}$), and S′ (Sb_2O_4) were mixed with ZnO at doping levels equivalent to 0.1 and 2.0 mol % of Sb_2O_3 under the same condition described above. The powder mixtures without binder were compacted uniaxially into discs of 1.0 cm^2 cross sectional area and 0.4 cm thick. The compacting pressure was adjusted between 19.6 and 30.4 MPa to ensure the same green density of 3.00 $\pm$ 0.02 g cm^{-3}.

2.2. Procedures

The linear shrinkage was determined with a dilatometer (ULVAC DL-500 Sinku-Rico Co.) at a heating rate of 300° C h^{-1} in air. Powder compacts were preheated to oxidize Sb_2O_3 at 500° C for 1 h, and then fired between 700° C and 1400° C for 1 h by fast firing in air. The fired densities were determined by the water-immersion method. Samples were polished and etched thermally between 970° C and 1050° C for microstructure observation. Samples with less than 70% of theoretical densities were impregnated with epoxy resin in a vacuum chamber and polished. Microstructures were examined by SEI (Second Electron Image) and BEI (Back-Scattered Electron Image) of SEM (JSM-T100, JEOL). Phases in the sintered specimens were identified by X-ray powder diffraction analysis (CN-2103, Rigaku Electric Co.) using Cu$K\alpha_1$ radiation.

3. Results and discussion

3.1. Effect of Sb_2O_3 on densification

Fig. 2 shows the densification characteristics of the specimens containing up to 2.0 mol % coarse Sb_2O_3 (designated as ZS_cX, where X is the mole percent of Sb_2O_3). Pure ZnO starts shrinking at about 600° C and completes densification at about 1100° C. Addition of

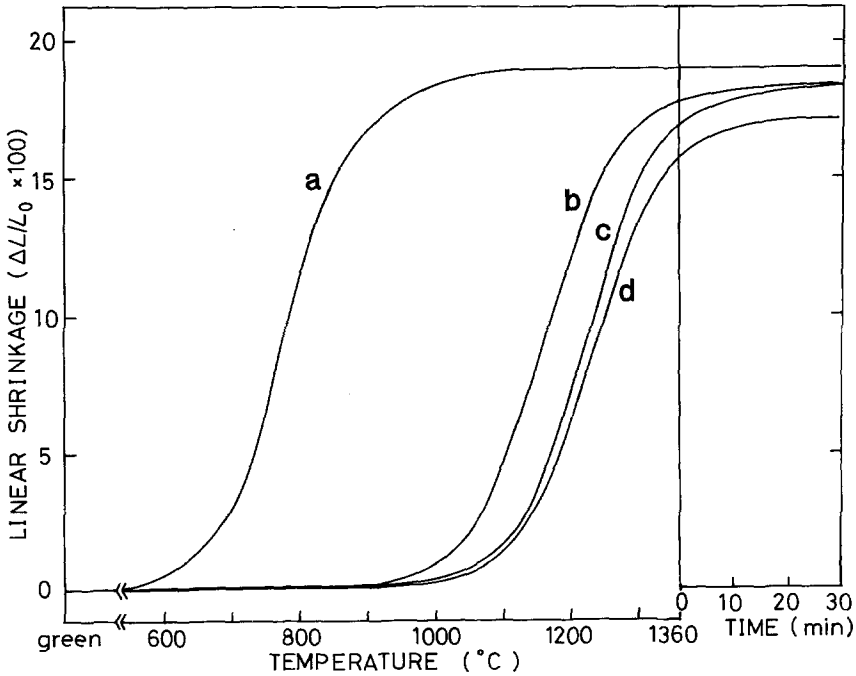

Figure 2 Effect of Sb_2O_3 (coarse) on the densification characteristics of ZnO. (a) No addition, (b) 0.1, (c) 0.5 and (d) 2.0 mol %, heated at 5° C min^{-1}.

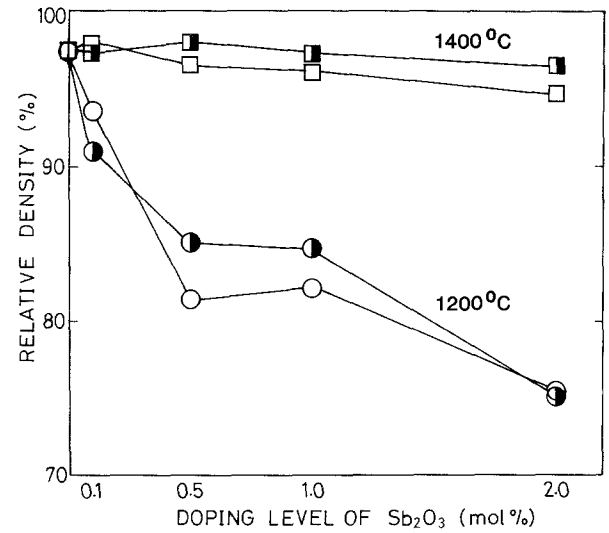

Figure 3 Effect of doping level of Sb_2O_3 on the density, heated for 1 h (○, □; ZS_c, ◑, ◨; ZS_f).

0.1 mol % Sb_2O_3, however, suppresses densification appreciably, and raises the densification temperature by 400° C. This is consistent with the result of Trontelj *et al.* [5]. No significant effect of doping level on the densification was observed. Thus, an increase in the doping level from 0.1 to 2.0 mol % increased the densification temperature by 60° C. Similar densification characteristics were obtained with fine Sb_2O_3 (S_f), but the final shrinkage was larger than that for coarse Sb_2O_3 (S_c).

Fig. 3 shows the effect of doping level on the fired density for ZS_cX and ZS_fX. In both cases, the fired density decreased with increasing doping level, and the effect of doping level was less significant at high temperatures. Above 1200° C, ZS_fX gave higher densities than ZS_cX.

3.2. Effect of chemical species of Sb_2O_3 on densification

Three different chemical species of antimony oxide, Sb_2O_4, $ZnSb_2O_6$ and α-$Zn_7Sb_2O_{12}$, were added to ZnO at doping levels equivalent to 0.1 mol % Sb_2O_3 (ZS'0.1, ZZS0.1 and ZSP0.1, respectively) and compacted into discs. Fig. 4 illustrates their densification characteristics. Densification of ZnO containing three antimony additives is in good contrast to that of ZS_c0.1. The densification starts at about 600° C just like pure ZnO, and proceeds at a much lower rate till 1100° C. Above 1100° C, all the doped specimens exhibit almost the same densification characteristics. For doping levels equivalent to 2.0 mol % Sb_2O_3, no significant difference in densification was observed among specimens containing different chemical species of antimony.

Fig. 5 shows the micrographs of the fracture surfaces of ZS_c0.1 and ZSP0.1 sintered at 800° C for 1 h. In ZSP0.1, coarsening due to neck growth between ZnO particles has occurred, while ZS_c0.1 showed no evidence of coarsening with the particle size of ZnO almost the same as that of the green compact. This difference will be explained later in this paper referring to the interaction between additives and ZnO.

3.3. Phase changes in antimony-doped ZnO

In order to understand the densification characteristics of Sb_2O_3-doped ZnO, phase changes during heating were studied by XRD. Effect of $ZnSb_2O_6$ and Sb_2O_4 addition on the phase change was studied also. The doping level of different additives was equivalent to 2.0 mol % Sb_2O_3 for all specimens.

Fig. 6 illustrates the diffraction patterns of ZS_c2.0 fired at various temperatures. No reaction between ZnO and Sb_2O_3 occurs up to 400° C. Between 500 and 800° C, ZnO is the only crystalline phase and a halo appears in the low angle range. The crystalline phase of α-Zn_7Sb_{12} appears at 900° C. Isothermal heating of ZS_c2.0 at 900° C for 10 min gave 80% yield in the formation of α-$Zn_7Sb_2O_{12}$. The beta $Zn_7Sb_2O_{12}$ phase was observed at 1200° C, which transformed into α-$Zn_7Sb_2O_{12}$ above 1300° C. Heat treatment of pure α-$Zn_7Sb_2O_{12}$ showed that the α–β transformation between 1200 and 1300° C is reversible, but that β-$Zn_7Sb_2O_{12}$ does not transform into α-$Zn_7Sb_2O_{12}$ below 1200° C. Thus, α-$Zn_7Sb_2O_{12}$ observed in ZS_c2.0

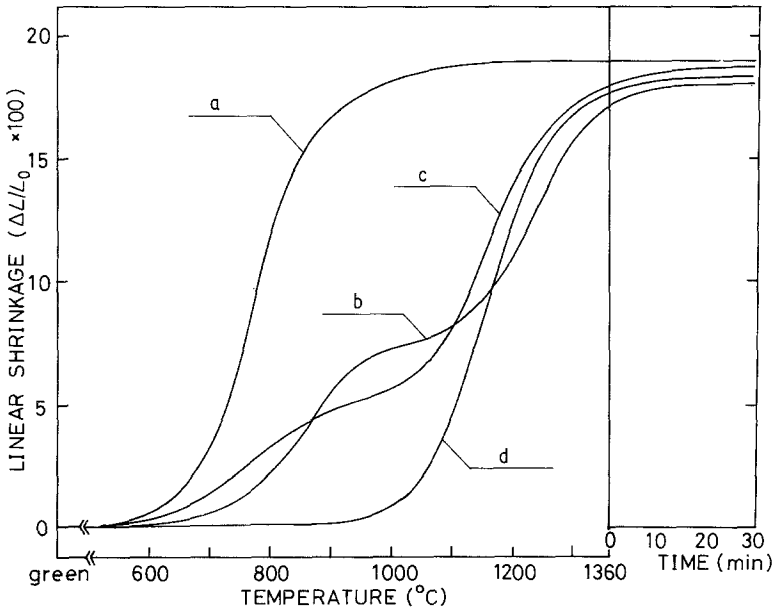

Figure 4 Effect of antimony-dopant on the densification characteristics of ZnO. (a) ZR; no addition, (b) ZS'0.1; Sb_2O_4 (c) ZZS0.1 and ZSP0.1; $ZnSb_2O_6$ and α-$Zn_7Sb_2O_{12}$, respectively and (d) coarse Sb_2O_3. Doping level equivalent to 0.1 mol % Sb_2O_3, heated at 5° C min^{-1}.

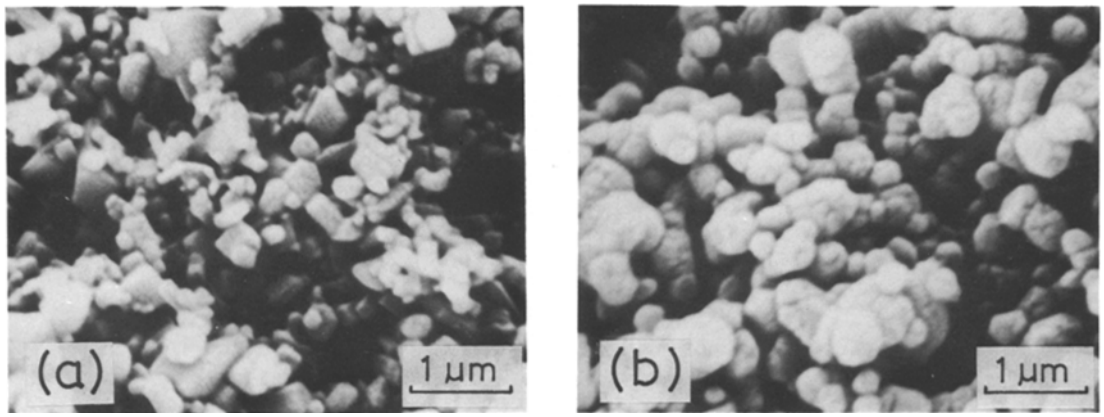

Figure 5 Effect of dopant on the sintering of ZnO particles, heated at 800° C for 1 h. (a) Coarse Sb_2O_3, (b) α-$Zn_7Sb_2O_{12}$, each equivalent to 0.1 mol % Sb_2O_3.

below 1200° C is probably unstable. Phase changes in $ZS_f2.0$ were almost the same as those in $ZS_c2.0$ in the temperature range studied, implying that the phase changes are not sensitive to the particle size of dopant Sb_2O_3.

The diffraction patterns of ZS′2.0 and ZZS2.0 sintered at the same temperature as $ZS_c2.0$ are illustrated in Fig. 7. In both cases, no phase changes are observed till 700° C. In ZS′2.0, a new phase $ZnSb_2O_6$ appears at 800° C at the expense of Sb_2O_4, and transforms into α-$Zn_7Sb_2O_{12}$ at about 900° C. The formation reaction of α-$Zn_7Sb_2O_{12}$ is sluggish as compared with that of $ZS_c2.0$, so that the phase $ZnSb_2O_6$ remains in the sample sintered at 1000° C for 1 h. In ZZS2.0, α-$Zn_7Sb_2O_{12}$ appears at 900° C, and the phase $ZnSb_2O_6$ disappears completely to change into β-$Zn_7Sb_2O_{12}$ at 1000° C.

Since there were no indications of line broadening or peak shifts of ZnO in $ZS_c2.0$ fired at various temperatures, Sb_2O_3 at doping levels up to 2.0 mol % should react directly with ZnO without forming a solid solution. Probably, doped Sb_2O_3 exists as a non-crystalline phase of an unknown composition between 500° C and 800° C. This non-crystalline phase in Sb_2O_3-doped ZnO changes directly into α-$Zn_7Sb_2O_{12}$, while $ZnSb_2O_6$ appears before the formation of α-$Zn_7Sb_2O_{12}$ in Sb_2O_4-doped ZnO. The difference in phase changes between Sb_2O_3-doped ZnO and ZnO doped with the other antimony oxides is due to the behaviour of Sb_2O_3 on heating, which is responsible for the retardation of densification of Sb_2O_3-doped ZnO.

Zinc oxide doped with α-$Zn_7Sb_2O_{12}$ exhibited no phase change other than α–β transformation of $Zn_7Sb_2O_{12}$ between 1200° C and 1300° C.

3.4. Behaviour of Sb_2O_3 in ZnO

Results of dilatometry and XRD indicate that the densification characteristics of ZnO are modified considerably by Sb_2O_3 addition. So, the role of Sb_2O_3 in the sintering of Sb_2O_3-doped ZnO was studied.

Fig. 8 illustrates the results of DTA and TG of Sb_2O_3 and $ZS_c2.0$ in air. Pure Sb_2O_3 shows a sharp exothermic peak due to oxidation of Sb_2O_3 [20] at about 530° C. XRD studies revealed that Sb_2O_3

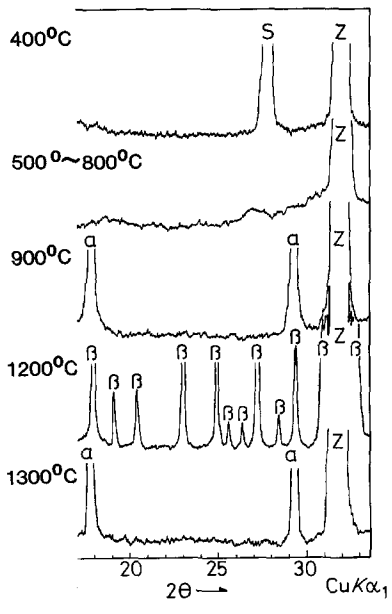

Figure 6 Phase changes in ZnO, doped with 2.0 mol % Sb_2O_3, heated for 1 h. Z; ZnO, S; Sb_2O_3, α; α-$Zn_7Sb_2O_{12}$, β; β-$Zn_7Sb_2O_{12}$.

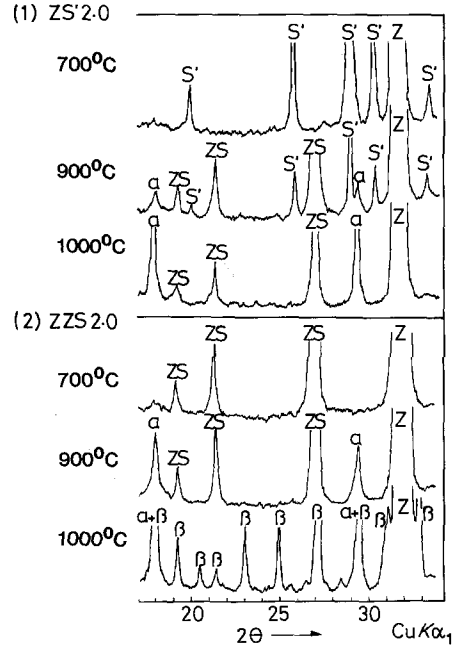

Figure 7 Effect of dopant on the phase change of ZnO, heated for 1 h, doping level equivalent to 2.0 mol % Sb_2O_3. S′; Sb_2O_4, ZS; $ZnSb_2O_6$. See Fig. 6 for phase identification.

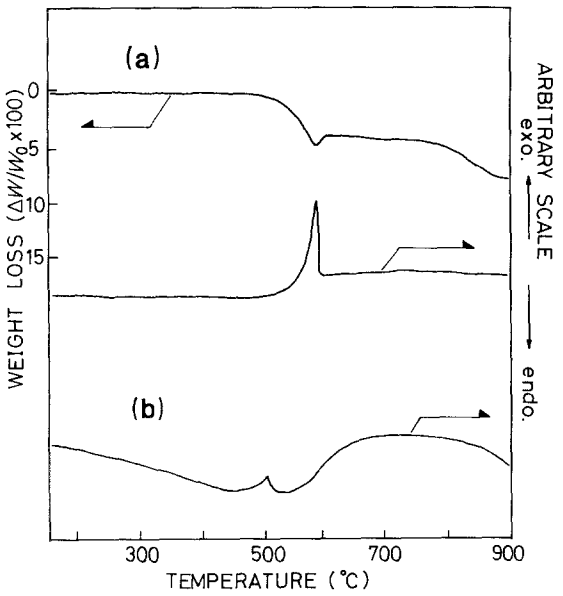

Figure 8 TG and DTAs of coarse Sb_2O_3 with and without ZnO. (a) Coarse Sb_2O_3, (b) 2.0 mol % coarse Sb_2O_3 in ZnO, heated at 10° C min^{-1}.

changes to Sb_2O_4 at 600° C and transforms into β-Sb_2O_4 at 900° C.

A large weight loss between 475 and 600° C is in discrepancy with what is expected from the sharp oxidation peak in DTA. Apparently, the volatilization of antimony oxide during oxidation is responsible for the observed weight loss. The gradual weight decrease above 700° C is probably explained by the decomposition of Sb_2O_4 [21]. The amount of Sb_2O_3 loss at 600° C calculated on the assumption that Sb_2O_3 has changed to Sb_2O_4 completely is less than 9 wt %.

Antimony trioxide in ZnO exhibited different behaviour during firing. Zinc oxide doped with 2.0 mol % Sb_2O_3 gave an exothermic peak at a temperature lower than that of pure Sb_2O_3, and showed a small weight increase roughly equivalent to that by the oxidation of doped Sb_2O_3 at 700° C when compacted into a disc. These results indicate that the vaporized antimony condenses on the ZnO particle surfaces as a non-crystalline phase or reacts with ZnO to form thin films of non-crystalline zinc antimonate below 900° C. Thus, the antimony-containing thin film on the ZnO particle surface suppresses the densification by hindering the material transport of ZnO (Figs 2 and 5). The similar densification characteristics for ZS_cX and ZS_fX and the rapid formation of α-$Zn_7Sb_2O_{12}$ in ZS_cX are in favour of this view. Above 900° C, α-$Zn_7Sb_2O_{12}$ forms and grows to inclusion particles on the grain boundaries of ZnO.

Fig. 9 shows BEIs of $ZS_c0.5$ and $ZS_f0.5$ sintered at 1200° C for 1 h. Inclusion particles of submicron sizes are dispersed uniformly in the ZnO matrix regardless of the particle size of Sb_2O_3. Thus, the coating of ZnO particles with antimony oxide and subsequent reaction to form α-$Zn_7Sb_2O_{12}$ are plausible explanations for the observed behaviour of Sb_2O_3. If α-$Zn_7Sb_2O_{12}$ forms at the contact areas between Sb_2O_3 and ZnO particles, the size of inclusion particles should depend on the particle size of Sb_2O_3.

3.5. The effect of Sb_2O_3 particle size on pore structure in Sb_2O_3-doped ZnO

Fig. 10 shows microstructures of ZnO containing 2.0 mol % Sb_2O_3 fired at 700° C. In ZnO containing coarse Sb_2O_3, large pores develop and remain on further heating. In ZnO containing fine Sb_2O_3, on the other hand, only small pores are observed. The number of large pores increased with increasing coarse Sb_2O_3 content resulting in lower densities than ZS_fX for all the doping levels studied. Probably, these pores were generated by the vaporization of Sb_2O_3 particles.

To understand the interaction between ZnO and Sb_2O_3, a mixture of ZnO granules and 0.5 mol % of Sb_2O_3 granules were compacted and fired at various temperatures, and the microstructure was observed. The same experiment was made for a mixture of ZnO granules and 0.5 mol% of Sb_2O_4 granules for comparison. Fig. 11 shows BEIs of these samples. In $ZS_c0.5$, the porous areas partly filled with an antimony-rich phase develop at 700° C. Above 900° C, the non-crystalline phase around the porous areas reacts with ZnO to form α-$Zn_7Sb_2O_{12}$. These situations are well illustrated in Figs 11a and b.

In ZS'0.5, on the other hand, granules of Sb_2O_4 exist without any reaction at 700° C. Antimony tetraoxide in these granules reacts with surrounding ZnO particles to form $ZnSb_2O_6$ and subsequently α-$Zn_7Sb_2O_{12}$ at higher temperatures. The shape and interfacial crack of a heterogeneous α-$Zn_7Sb_2O_{12}$ particle in the sample fired at 1400° C support this

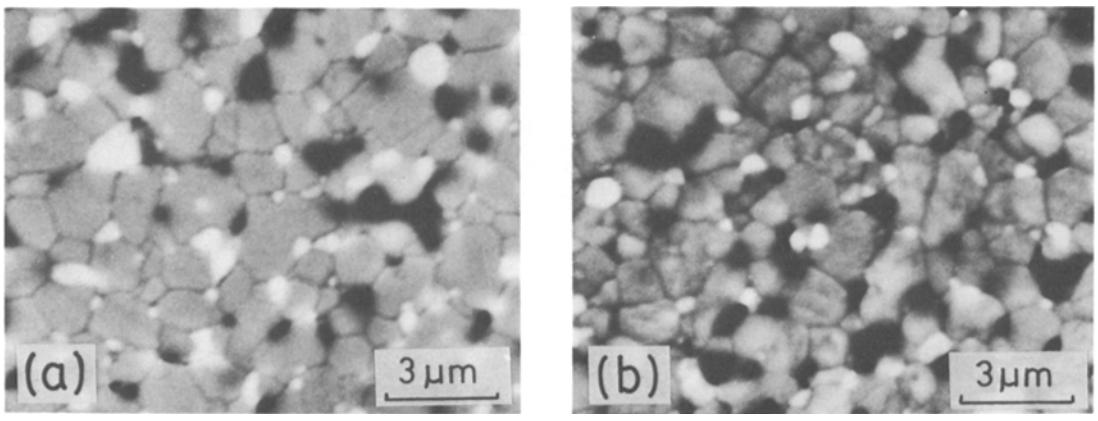

Figure 9 Effect of Sb_2O_3 particle size on the dispersion of α-$Zn_7Sb_2O_{12}$. (a) Coarse, (b) fine 0.5 mol % Sb_2O_3, heated at 1200° C for 1 h.

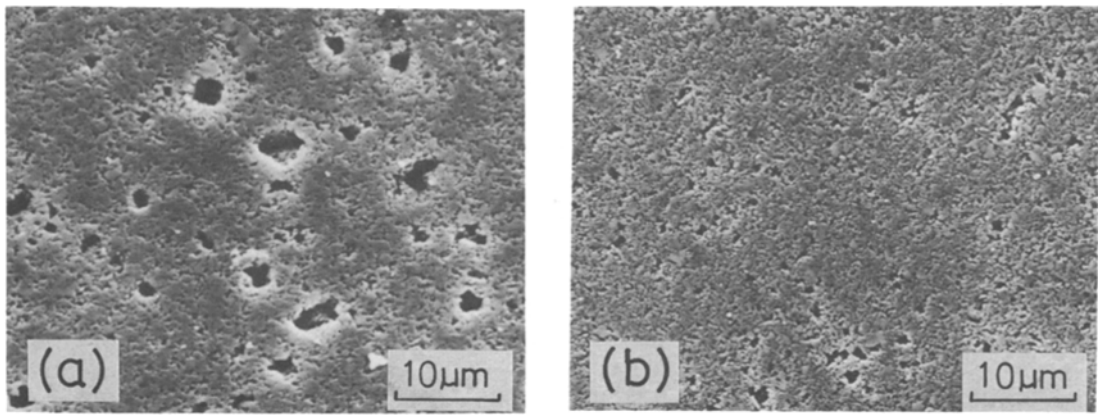

Figure 10 Effect of Sb_2O_3 particle size on the pore structure. (a) Coarse, (b) fine 2.0 mol % Sb_2O_3, heated at 700° C for 1 h.

view. These situations are illustrated in Figs 11c and d.

The difference in the behaviour of doped antimony-oxide is demonstrated in Fig. 11; doped Sb_2O_3 evaporates and condenses on ZnO particles. Other antimony oxides, on the other hand, react with surrounding ZnO to form inclusion particles of which size depends on the size of the antimony oxides.

4. Conclusion

Addition of Sb_2O_3 from 0.1 to 2.0 mol % raised the densification temperature of ZnO from 600° C to 1000° C regardless of the size and doping level of Sb_2O_3.

Addition of $ZnSb_2O_6$, α-$Zn_7Sb_2O_{12}$, and Sb_2O_4, however, gave densification characteristics different from Sb_2O_3-doped ZnO; a slight densification takes place at 600° C but the densification does not complete below 1200° C.

The densification characteristics in Sb_2O_3-doped ZnO have been explained as due to the volatile nature of Sb_2O_3. Thus, Sb_2O_3 evaporates during oxidation at about 500° C and condenses on ZnO particle surfaces as a non-crystalline phase of an unknown composition, which checks the material transport across ZnO particles resulting in the retarded densification.

Densification does not start until the antimony oxide film on ZnO particle surfaces is eliminated through the formation of crystalline α-$Zn_7Sb_2O_{12}$ at about 900° C and subsequent growth to fine inclusion particles at higher temperatures.

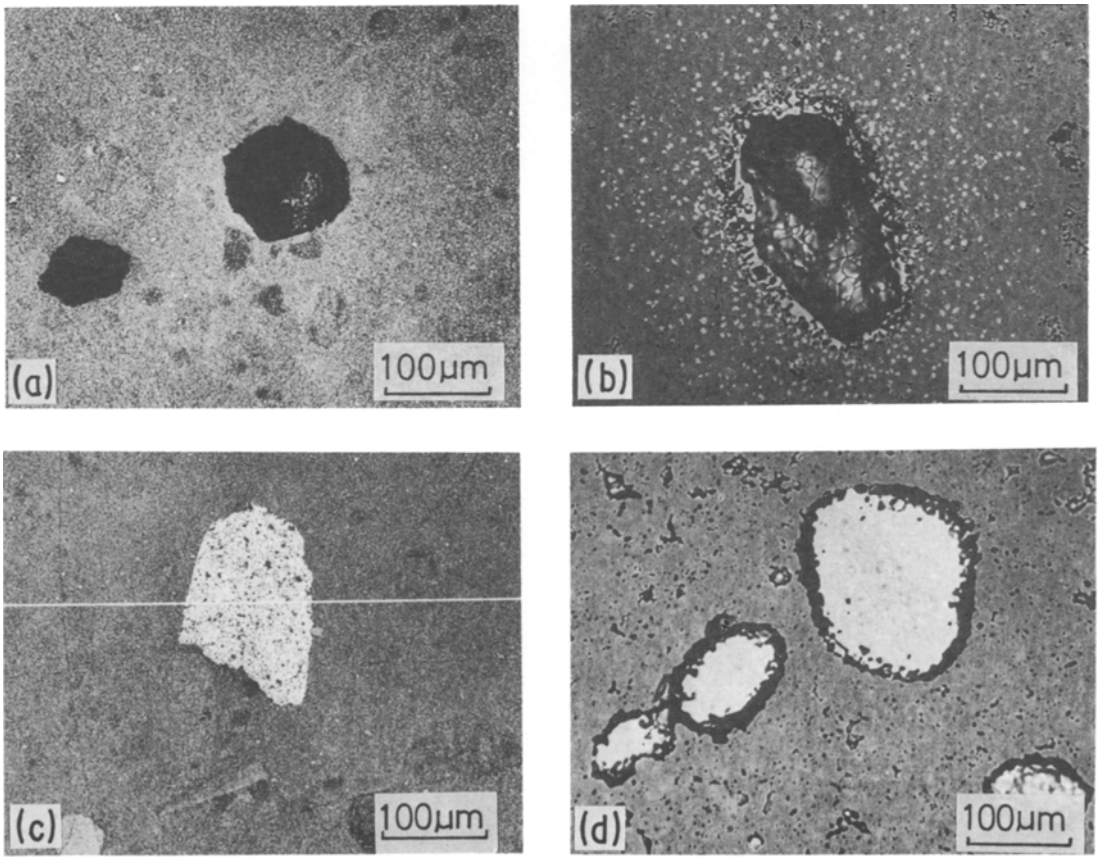

Figure 11 Micrographs illustrating the effect of evaporation on the microstructure of ZnO mixed with, (a) (b) granulated Sb_2O_3, (c) (d) granulated Sb_2O_4. Doping level equivalent to 0.5 mol % Sb_2O_3, heated at (a) (c) 700° C, and (b) (d) 1400° C for 1 h.

Acknowledgement

The authors express their appreciation to Dr H. Okuma of Toshiba Corporation for his assistance in executing this work.

References

1. T. SEIYAMA, A. KATO, K. FUJIISHI and M. NAGATANI, *Anal. Chem.* **34** (1962) 1502.
2. M. MATSUOKA, *Jpn J. Appl. Phys.* **10** (1971) 736.
3. L. M. LEVINSON and H. R. PHILIPPS, *ibid.* **46** (1975) 1332.
4. T. K. GUPTA, *J. Amer. Ceram. Soc.* **54** (1971) 413.
5. M. TRONTELJ and D. KOJAR, *J. Mater. Sci. Lett.* **13** (1978) 1832.
6. W. KOMATSU, H. OOKI, I. NAKA and A. KOBAYASHI, *J. Catalysis* **15** (1969) 43.
7. W. KOMATSU, M. MIY'AMOTO, S. FUJITA and Y. MORIYOSHI, *J. Ceram. Assoc. Jpn* **76** (1968) 407.
8. W. KOMATSU, Y. MORIYOSHI and N. SETO, *Yogyo-Kyokai-Shi* **77** (1969) 347.
9. C. S. SMITH, *Trans. AIME* **175** (1948) 15.
10. E. NES, N. RYUM and O. HUNDERI, *Acta. Metall.* **33** (1985) 11.
11. H. H. v. BAUMBACH and C. WAGNER, *Z. Phys. Chem.* **B22** (1933) 199.
12. K. HAUFFE and J. BLOCK, *ibid.* **196** (1950) 438.
13. A. T. SANTHANAM, T. K. GUPTA and W. G. CARLSON, *J. Appl. Phys.* **50** (1979) 852.
14. J. WONG, *ibid.* **46** (1975) 1653.
15. K.-H. BÄTHER, D. HINZ, N. MATTERN, M. BITTERLICH and W. BRÜCKNER, *Phys. Status Solidi (a)* **61** (1980) K9.
16. W. G. MORRIS, *J. Amer. Ceram. Soc.* **57** (1973) 360.
17. G. STANISIĆ, M. MILOSEVSKI and I. KRSTNOVIC, *Sci. Sintering* **16** (1984) 121.
18. M. INADA, *Jpn J. Appl. Phys.* **17** (1978) 1.
19. V. G. BAYER, *Ber. Dtsch. Keram. Ges.* **39** (1962) 535.
20. T. CARNELLEY and J. WALKER, *J. Chem. Soc.* **53** (1888) 86.
21. H. BAUBIGNY, *Compt. Rend.* **124** (1897) 499.

Received 16 December 1987
and accepted 27 April 1988